Proceedings of the 21st ICSMGE, Vienna, Austria, 14 – 19 June 2026. Pistrol, Adam & Schweiger (eds.)
Published by: ÖGG, Austrian Society for Geomechanics, Salzburg, Austria, ISBN 978-3-9503898-4-5
https://doi.org/10.53243/ICSMGE2026-1203

Experience with load-transfer method for analysis of deep foundation in the Czech Republic and Austria

Juraj Chalmovský, Jaroslav Havlíček
Institute of Geotechnics, Brno University of Technology, Czech Republic, xschalmovskyj@vutbr.cz

Václav Račanský, Martin Hayden
Keller Grundbau Ges.mbH, Austria

ABSTRACT: This paper summarizes the experience gained and subsequent modifications of the load-transfer method for ground anchors, bored piles, and driven piles, which have been performed over the last ten years at the Technical University of Brno. Fixed lengths of ground anchors have a high slenderness ratio, resulting in a non-uniform distribution of shaft friction and possible progressive failure. Therefore, a load-transfer function with post-peak softening was used. Additionally, an algorithm controlling the gradual reduction in axial stiffness owing to the occurrence of tensile cracks along the fixed length was implemented. In the case of bored piles, the β effective stress approach was embedded in the load-transfer method. This approach was further refined into three stages to cover a wider range of soil types. In the first stage, the β factor is constant, resulting in a linear dependence of the ultimate skin friction on the effective overburden stress. The second stage, applicable to overconsolidated cohesive soils, includes the dependence of the β factor on the depth and degree of overconsolidation. The third stage of analysis is extended to consider the increase in radial stresses during loading owing to the constrained dilatancy effect occurring in middle-dense to dense non-cohesive soils. Finally, the load-transfer method was adapted for ductile-driven piles. The time required for hammering each meter of pile was utilized to estimate the ultimate shaft friction using the load-transfer coefficients. All the theoretical concepts were tested via inverse analyses of multiple loading tests. To perform more analyses and obtain a more reliable library of inputs, the calculations were automated using a stochastic optimization algorithm.

KEYWORDS: Load-transfer method, piles, ground anchors, progressive failure, tension stiffening, effective stress approach, constrained dilatancy effect, optimization method

1 INTRODUCTION

The load-transfer method (LTM) is a popular design tool frequently used for design of axially and laterally loaded foundation elements and their groups. Introduced by Seed and Reese (1957), it has undergone extensive developments and improvements. Since the initial application for tension piles (Sulaiman & Coyle 1976; Reddy et al. 1997; Reddy et al. 1998), LTM was adopted for compression piles (Zhang & Zhang 2012), piles subjected to unloading-reloading cycles (Dias & Bezuijen 2018), rectangular closed form diaphragm walls (Wu et al. 2016), pile groups (Zhang et al. 2014) and energy piles (Sutman et al. 2018). LTM presents a certain compromise between complex numerical methods and analytical closed form solutions.

2 LOAD-TRANSFER METHOD

The axial load-transfer method is based on the idea that an axially loaded member (e.g. a tension or compression pile) can be divided into a finite number of segments which are each assigned a unique dependence between the vertical displacement of the segment (s_s) and the shear stress mobilized on its surface (q_s). The function is called the load-transfer (mobilization) function (curve). A similar dependency between the normal stress at the pile base (s_b) and the corresponding base displacement (s_b) is added for the pile tip in the case of compressive loads. The structural model of a pile analyzed using the load transfer method is shown in Figure 1. The equilibrium of forces acting on the lower and upper edge of the segment and the force due to skin friction acting on the shaft of the segment is solved for each segment. This equilibrium condition is supplemented by the force resulting from the mobilization of base resistance at the bottom edge of the last element. A feature of this approach is that the effect of overall pile stiffness (EA/L) on the vertical displacement and thus mobilized shaft friction along the pile is directly considered.

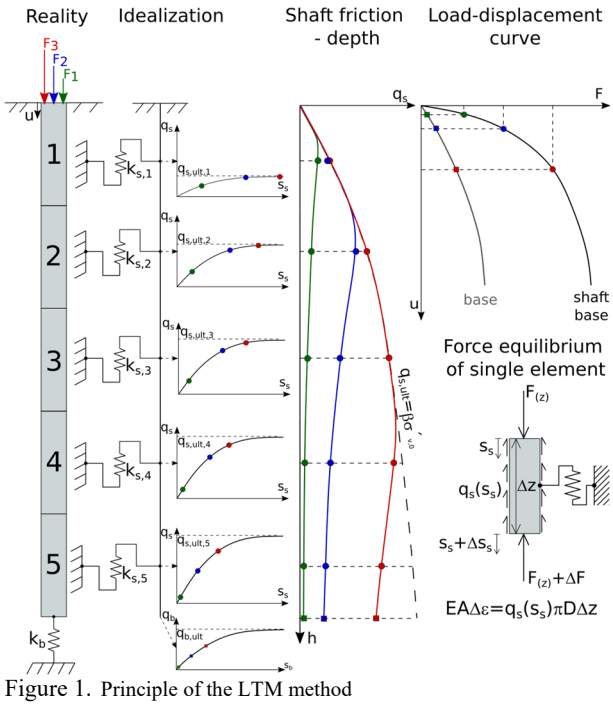

Figure 1. Principle of the LTM method

3 LTM MODIFICATIONS

3.1 *Ground anchors*

The ground anchors exhibit non-uniform skin friction mobilization due to the high slenderness ratio of a fixed length. In the first loading stages, mobilized shear stresses at the grout - soil interface are concentrated at the top of the fixed anchor length. After reaching the peak skin friction $q_{s,ult,p}$, shear stresses gradually drop towards the critical value $q_{s,ult,crit}$ and

the peak bond strength location moves along the fixed anchor length, as is schematically shown in Figure 2. This feature, known as the progressive failure phenomenon, has been studied by several authors e.g. Ostermayer (1975), Barley (1997), Wu *et al.* (2015), Vukotic et al. (2013).

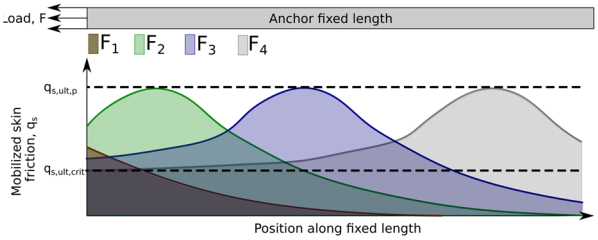

Figure 2. Progressive failure phenomenon

To include this phenomenon to analyses via LTM, the peak load transfer function proposed by Kraft et al. (1981) was utilized. The function is divided into two segments (Figure 3):

- The pre-failure segment: mobilized shear stress is increasing towards its peak value.
- The post-failure segment: mobilized shear stress is decreasing towards the critical state.

The vertical displacement s_s of each anchor segment during hardening is governed by Equation (1), where q_s is the shear stress mobilized on the segment surface with the radius of r_0, $q_{s,ult,p}$ is the peak bond strength, R_f is the stress-strain curve-fitting constant, G_i is the initial shear modulus and r_m is the radius of the zone influenced by anchor loading. The concentric cylinder approach proposed by Randolph and Wroth (1978) is combined with a non-linear (hyperbolic) expression of soil stress-strain behavior in this equation.

$$s_s = \frac{q_s r_0}{G_i} \ln \frac{\frac{r_m}{r_0} - \frac{q_s R_f}{q_{s,ult,p}}}{1 - \frac{q_s R_f}{q_{s,ult,p}}} \qquad (1)$$

It is not possible to apply Equation (1) to the post-failure segment of the load-transfer function due to the development of slip surfaces directly on the fixed length surface (the grout-soil interface) or in its vicinity (the soil-soil interface). Kraft et al. (1981) proposed constructing the post-failure segment of the load-transfer function using the direct shear test. Displacements δ_z measured during laboratory tests (Fig. 2) are adjusted by the elastic rebound Δz_e (snap-back) occurring in the soil beyond the slip surface due to unloading in the post-failure regime. Corrected displacements Δz and corresponding values of shear stress are then used in the load-displacement curves.

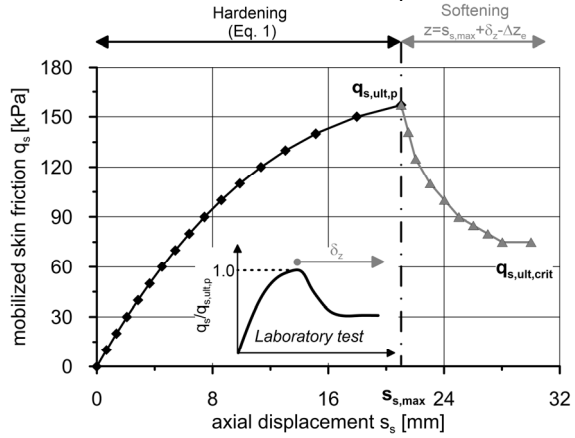

Figure 3. Post-peak load-transfer function

To predict anchor head displacements during loading more correctly, it is necessary to consider the gradual decrease in the axial stiffness of the tendon-grout system due to the occurrence of tensile cracks in the grout. This mechanism is similar to the tension stiffening of a concrete beam with a centrally placed reinforcement. A schematic load-displacement curve for such a beam is shown in Figure 4.

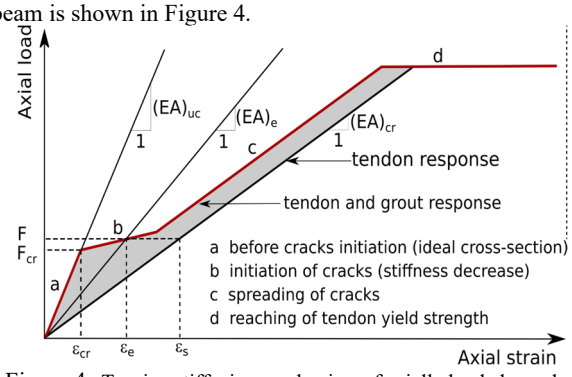

Figure 4. Tension stiffening mechanism of axially loaded member

During the initial stages of loading, both the tendon and the grout contribute to the overall "uncracked" axial stiffness EA_{uc}. After reaching the critical force F_{cr} corresponding to the strain ε_{cr}, tensile cracks start to develop, and the stiffness contribution of the grout material gradually decreases. The overall axial stiffness approaches the tendon stiffness EA_{cr}. The proposed procedure offers three possible alternatives after grout tensile strength is reached. The simplest of these is to instantly neglect the grout stiffness after the axial strain limit corresponding to the grout tensile strength is reached. Alternatively, the analytical formulations of tension stiffening stated in the CEB-FIP Model Code 1990 (1993) and ACI 318 (2014) are incorporated in the application. The modulus of elasticity is gradually reduced in the former, the ideal cross-sectional area is adjusted in the latter.

3.2 *Bored piles*

The hyperbolic load-transfer curves for the shaft (Equation 2) and the base (Equation 3) proposed by Bohn et al. (2016) were utilized for piles. The initial stiffness of the load-transfer curves is governed by M_s and M_b variables for the pile shaft and base, respectively. The ultimate pile shaft resistance ($q_{s,ult}$) and the bearing capacity of the pile base $q_{b,ult}$ represent the asymptotic stress states, D_s and D_b are the diameter of the pile shaft and base, respectively. The load transfer functions for various $q_{s,ult}/M_s$ ratios are shown in Figure 5.

$$q_s = \frac{q_{s,ult} s_s}{M_s D_s + s_s} \qquad (2)$$

$$q_b = \frac{q_{b,ult} s_b}{M_b D_b + s_b} \qquad (3)$$

The ultimate skin friction value is the governing input parameter in case of floating piles. Generally, it depends (Equation 4) on the friction angle on the shaft – soil interface (δ), the initial lateral stress on the pile surface ($\sigma'_{h,0}$), and on the lateral stress changes during construction ($\Delta\sigma'_{h,c}$) and loading ($\Delta\sigma'_{h,l}$). The change in lateral stress due to construction of bored piles is smaller compared to the displacement piles and is not considered here.

$$q_{s,ult} = \left(\sigma'_{h,0} + \Delta\sigma'_{h,c} + \Delta\sigma'_{h,l}\right) \tan\delta \qquad (4)$$

The effective stress approach (further noted as β method) relates the ultimate skin friction $q_{s,ult}$ to the soil effective stress state $\sigma'_{v,0}$ (Equation 5) as shown schematically in Figure 6.

$$q_{s,ult} = \beta \sigma'_{v,0} \qquad (5)$$

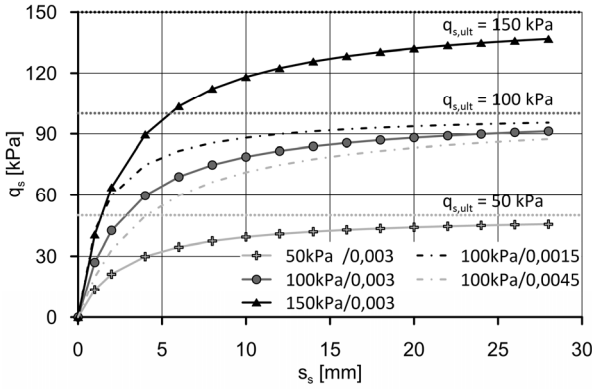

Figure 5. Hyperbolic load-transfer functions

Combining Equation (4) and (5) and assuming that $\sigma'_{h,0} = K_s\sigma'_{v,0}$ in Equation (4) yields:

$$\beta = \left(K_s + \frac{\Delta\sigma'_{hc}}{\sigma'_{v,0}} + \frac{\Delta\sigma'_{h,l}}{\sigma'_{v,0}}\right)\tan\delta \qquad (6)$$

where K_s is the earth pressure coefficient. The β method implemented in the LTM algorithm is further refined into the following three stages:

- Stage I – constant β factor, constant radial stress,
- Stage II – depth-dependent β factor, constant radial stress,
- Stage III – depth-dependent β factor, variable radial stress.

Stage I is appropriate mainly for piles in normally consolidated cohesive soils. Assuming that $\delta = \phi_{cv}$ and K_s equals to the coefficient of earth pressure at rest $K_s = K_0 = 1 - \sin\phi_{cv}$, β_I might be calculated from

$$\beta_I = (1 - \sin\varphi_{cv})\,tan\varphi_{cv} \qquad (7)$$

where ϕ_{cv} is the constant volume friction angle. The typical values of the factor β_I are in the range of 0.2 to 0.4.

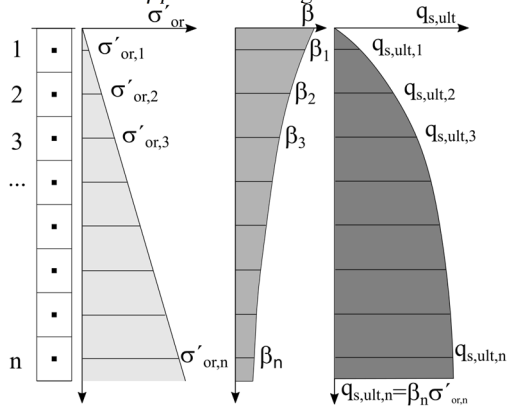

Figure 6. Effective stress dependent ultimate shaft friction

Burland (1973) recognized that the β factor is not constant in cohesive overconsolidated soils as the K_0^{oc} varies with depth. Therefore, the β_{II} is introduced in Equation (8). POP is the pre overburden pressure which states the difference between the past maximum effective vertical stress σ'_p and current effective vertical stress $\sigma'_{v,0}$.

$$\beta_{II} = (1 - \sin\varphi_{cv})\left(\frac{POP}{\sigma'_{or}} + 1\right)^{\sin\varphi_{cv}} \tan\varphi_{cv} \qquad (8)$$

In the first two analysis stages, constant radial stress during the pile loading is assumed ($\Delta\sigma'_{h,l} = 0$). This is a reasonable assumption for piles in cohesive soils, however in case of piles in non-cohesive soils the acting radial stress increases due to the constrained dilatancy effect (Figure 7) During loading, the pile experiences vertical movements s_s and consequently shear strains γ_s occur within a thin shear zone at the soil – pile interface. Subsequently, dilatancy and thus radial movements u_r occur in this zone. The increase in soil volume in the shear zone is partially restricted by the surrounding soil, and therefore an increase in radial stresses $\Delta\sigma'_{h,l}$ and consequently in the ultimate shaft friction take place.

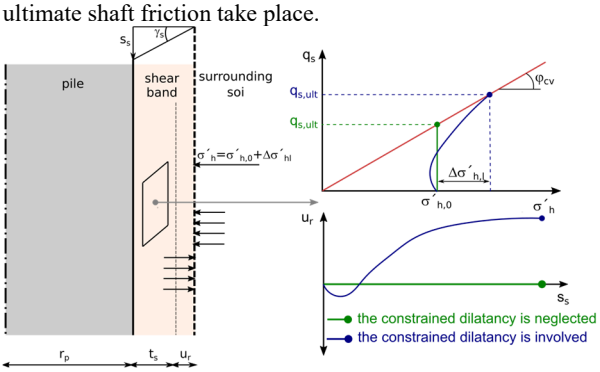

Figure 7. Constrained dilatancy effect

The β_{III} factor then reads:

$$\beta_{III} = \left((1 - \sin\phi_{cv}) + \frac{\Delta\sigma'_{h,l}}{\sigma'_{v,0}}\right) tan\varphi_{cv} \qquad (9)$$

$\Delta\sigma'_{h,l}$ is obtained assuming an elastic expansion of the cylindrical cavity (Equation 10), where G is the shear modulus, u_r is the radial movement and r_p is the pile radius, $k_n = G/2r_p$ is the radial stiffness. The procedure proposed by Lehane et al. (2005) is used to estimate u_r.

$$\Delta\sigma'_{h,l} = 2G\frac{u_r}{r_p} \qquad (10)$$

3.3 *Driven ductile iron piles*

The same type of hyperbolic-load transfer functions as for bored piles is utilized. However, due to the displacement nature of this technology, it is not possible to use three previously described stages of the β method. Instead, the ultimate shaft and base resistances are obtained according to Equation 11 and 12. HT_{shaft}^{ref} and HT_{base}^{ref} are the reference times required for hammering of each meter and the last 10 cm of pile, respectively.

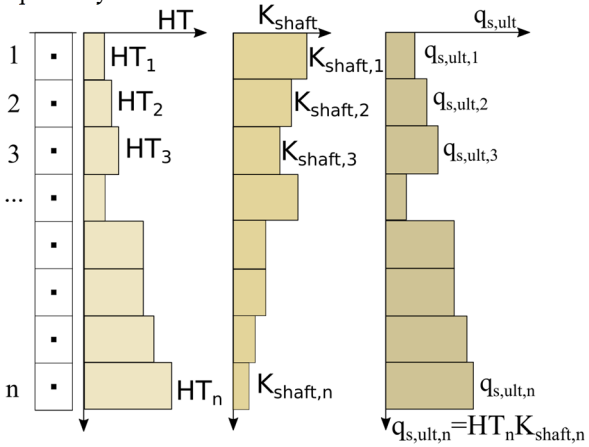

Figure 8. Hammering time dependent ultimate shaft friction

K_{shaft} and K_{base} are newly introduced load-transfer factors, the values of which depend on soil type and soil state.

$$q_{s,ult} = HT_{shaft}^{ref}K_{shaft} \qquad (11)$$

$$q_{b,ult} = HT_{base}^{ref}K_{base} \qquad (12)$$

Three groups of soils are distinguished in this approach: cohesive, cohesionless – sands, cohesionless – gravels. The soil state is reflected in hammering times as it requires longer time to hammer the pile in stiff/dense soils compared to soft/loose soils. Based on inverse analysis of more than 40 loading tests,

the nonlinear dependencies between the hammering time and load-transfer factors were established.

3.4 *Automation of LTM analyses via stochastic search algorithm*

To find the values of input parameters of the load-transfer functions more precisely, the LTM algorithm was combined with a stochastic optimization method. The genetic algorithm (Goldberg, 1989), further noted as GA was used. In the first step, a member represented by values of input parameters is binary coded. Each binary string (chromosome) consists of a predefined number of bits (genes). The length of the chromosome (the number of genes) depends on the number of input parameters and the required number of levels of each parameter. For example, if a pile is situated in a single geological layer and loaded by tension, two input parameters are required: the ultimate shaft friction $q_{s,ult}$ and the shaft stiffness parameter M_s. 64 possible levels of each parameter would require a binary string consisting of 12 bits. Three basic operations with created binary strings are involved in GA: reproduction, crossover and mutation. The primary objective of the reproduction operator is to increase the number of members with above-average fitness values. The binary tournament selection operator was used for this purpose. The crossover and mutation operators manipulate the binary coding of the chosen members and thus create new solutions and maintain their diversity. The single-point crossover operator, in which segments of binary strings are exchanged between two solutions, has been adopted. The number of solutions used in the crossover is governed by the crossover probability p_c. The mutation operator changes the value of only one bit (gene) at a position with a small mutation probability p_m. Finally, a new generation of members is created. Every member represents an input in the LTM analysis, after which the fitness value with measured data is evaluated and the whole process is repeated until a prescribed (minimum) value of the objective function is reached. Further details about the implementation of GA in LTM might be found in Chalmovsky (2024).

4 SELECTED CASE STUDIES

4.1 *Ground anchors*

The investigation loading test of the prestressed ground anchor constructed in stiff overconsolidated clays is analyzed via LTM. The test took place in the city of Brno, Czech Republic as a part of bigger testing site organized by the author´s home institution. The fixed length (L_{fixed}) of the analyzed anchor was 10m. To assess the mobilized skin friction, it was equipped by electric resistance gauges located on the tendon every two meters. The computations were performed with the following inputs: constant volume friction angle $\varphi_{cv} = 19.9°$, peak strength parameters $c_p = 90$ kPa and $\varphi_p = 14°$, fixed length diameter $d_{fixed} = 250$ mm, grout tensile strength $f_t = 2\ MPa$. Further details might be found in Chalmovsky and Mica (2020). The predicted and measured load-displacement curves are shown in Figure 9. The prediction yields slightly stiffer response, however, the ultimate carrying capacity is predicted with a reasonable accuracy. The shear stress and axial force distributions along the fixed length are plotted for multiple loading stages in Figure 10 and 11, respectively. At a load level of 900kN (86% of the ultimate carrying capacity), skin friction of less than 80kPa (42% of the ultimate bond strength) is mobilized at the distant end. This only emphasizes the necessity of involving non-linear soil stress-strain behavior in anchor design. At the ultimate state (1050kN), more than 4m of the fixed length is in the post-failure regime.

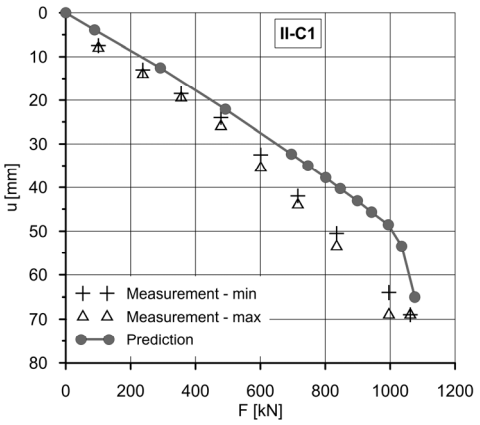

Figure 9. The load-displacement curve of anchor with L_{fixed}=10m

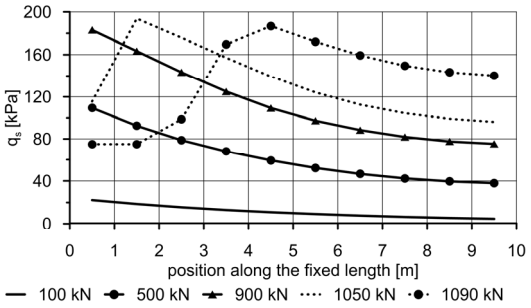

Figure 10. Shear stress distributions along fixed length

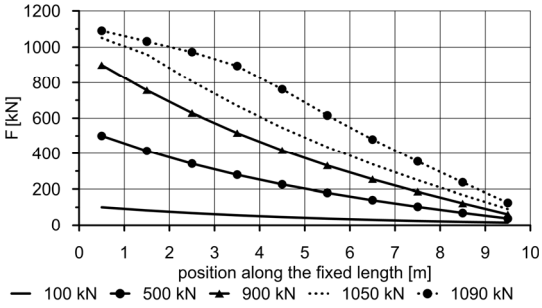

Figure 11. Axial force distributions along fixed length

Finally, the shear stress distribution in the ultimate state is compared with the distribution derived from measurement by electric resistance gauges (Figure 12). Three gauges were probably damaged during the post-grouting of the anchor. The non-linear shear stress distribution combined with the decrease in post-failure stress in the near section was observed. The predicted peak bond strength is 20kPa larger than the measured one and their locations differ by 2 meters with the experimentally observed post-peak section longer than the predicted one.

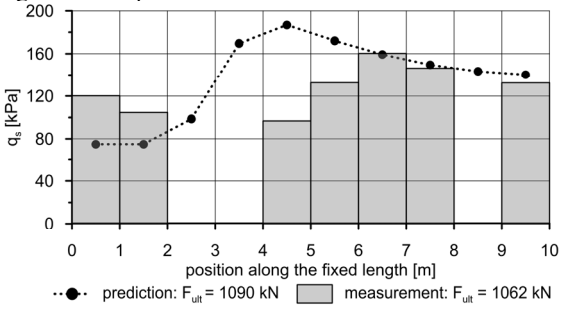

Figure 12. Predicted and measured shear stress distributions in the ultimate state

4.2 *Bored piles*

The loading tests of three bored piles are presented here. The first two test piles were constructed and tested (Figure 13) in the industrial zone near the city of Ostrava in the north-east part of the Czech Republic.

Figure 13. Pile load test arrangement

The upper 10.5 m of Quaternary silty clay with local lens of gravelly clay is underlained by Tertiary overconsolidated clay with a stiff to hard consistency with a CPT end resistance gradually increasing from 6 to 10 MPa. The Stage I and Stage II approaches were applied for the first and second layer, respectively. The $\beta_I = 0.27$ for the first layer was determined from Equation 7 assuming that $\phi_{cv} = 27°$. The computed ($M_s^1 = 0.0014$, $POP^2 = 1504\ kPa$, $M_s^2 = 0.0021$, $q_{b,ult} = 6000kPa$, $M_b = 0{,}031$, where the upper index indicates the layer number) and measured load-displacement curves for both piles are compared in Figure 14a. The ultimate shaft friction and corresponding β values are shown in Figure 14b.

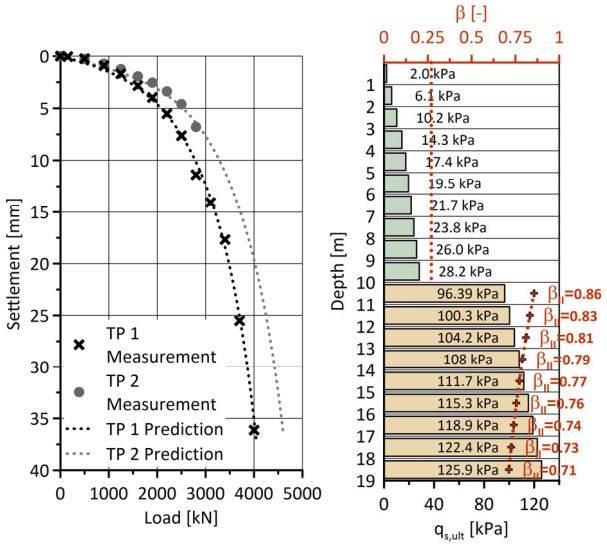

a) Load-displacement curve b) Ultimate shaft friction

Figure 14. Load tests of two bored piles in cohesive soils

The third pile load test analyzed in this study was performed in the city of Vienna as a part of the research project (Dietmar, 2020). The pile with a length of 6 m was constructed in middle dense to dense fluvial gravels of Quaternary age. Thus, the engineering-geological conditions are substantially different from those presented in the previous two piles. Stage III LTM analysis was carried out considering an increase in radial stress due to the constrained dilatancy effect. The values of input parameters used for the calculation shown in Figure 15 are as flows: $\phi_{cv} = 39°$, $\sigma_{hl} = 565\ kPa$, $M_s = 0.0394$.

4.3 *Driven piles*

Results from two loading tests are presented here. Two ductile piles, each 9 meters long, were constructed near the village of Hollern. The predominant soil type along the piles was clay with stiff consistency and both test piles were equipped with conical driving shoes. Even though they were constructed close to each other, different hammering profiles were recorded as shown in Figure 16. Generally, shorter hammering times were recorded for the pile PP3b and no hammering occurred in depths between 3 and 5 meters (the pile was only pushed downwards as the soil provided not enough resistance for hammering).

The assumed ultimate skin friction profiles are also plotted in Figure 16. The load-displacements curves for both piles are compared in Figure 17. The measured points correspond to the ends of the observation intervals of each loading stage after the acceptance criteria were met.

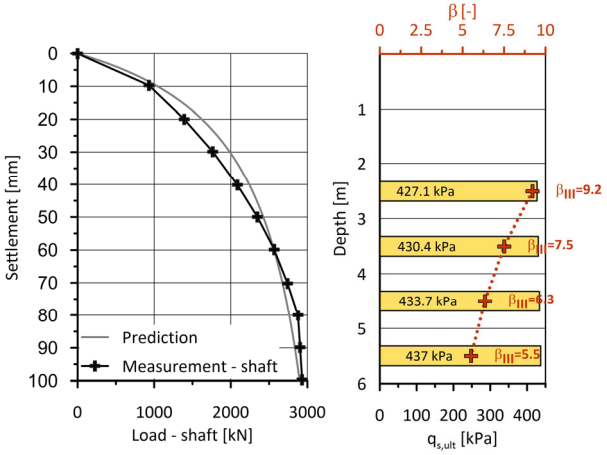

a) Load displacement curve b) Ultimate shaft friction

Figure 15. Load test of a pile in non-cohesive soils

The measured displacement values did not stabilize in the last loading stage. Therefore, the initial measured displacement value and value of 25 mm are both plotted for this loading stage. Shorter hammering times and thus lower values of the ultimate shaft friction resulted in worse response of the pile PP3b both in terms of the axial stiffness and the ultimate carrying capacity.

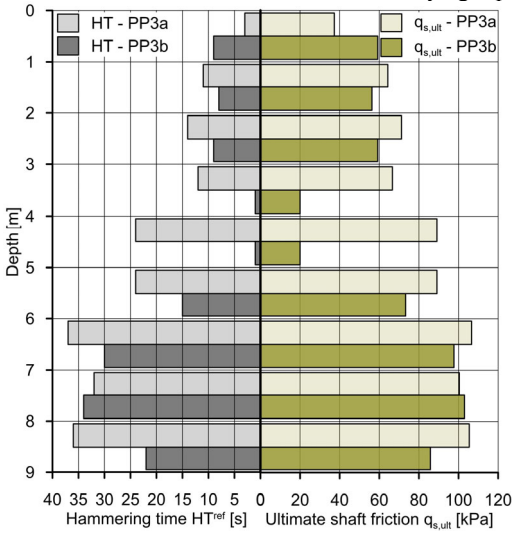

Figure 16. Profiles of hammering times and ultimate shaft friction for both tested piles

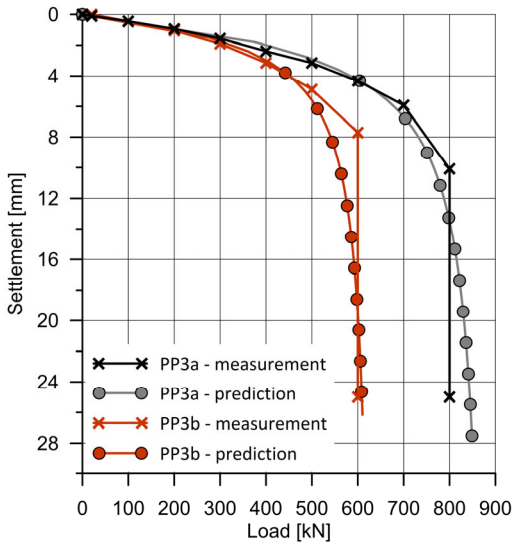

Figure 17. Profiles of hammering times and ultimate shaft friction for both tested piles

5 CONCLUSIONS

The paper presents the application and partial improvements of the load-transfer method for three types of geotechnical structures, namely ground anchors, bored piles and driven ductile piles.

The non-linear load-transfer function with the post peak strain softening was implemented to account for the non-uniform skin friction distribution and progressive failure mechanism in case of ground anchors. The combined axial stiffness of the tendon and surrounding grout is also considered. The gradual reduction of this stiffness due to the occurrence of tensile cracks in the grout material is implemented. This results in less uniform skin friction profiles and thus higher predicted displacements.

In case of bored piles, the effective stress (β) approach used for determination of the ultimate skin friction profiles was utilized. Three stages of this approach were distinguished to cover various types of soil. The first and second stages are appropriate for normally and ovreconsolidated cohesive soils, respectively. The case study of two loading tests in such geological conditions is presented in the paper. Finally, the third stage considers the constrained dilatancy effect due to which significantly higher shaft frictions are mobilized in coarse-grained soils.

The fact that hammering time profiles are recorded routinely during installation of ductile driven piles is used. The non-linear expression between the reference hammering time and the ultimate skin friction was established for three soil types based on multiple inverse analysis of filed tests. The field test of two piles with highly different recorded hammering times is presented.

The load-transfer method is an efficient design tool. If it is supplemented by a library or recommendations for a proper choice if its input parameters, it provides sufficiently accurate analyses of various types of geotechnical structures.

6 ACKNOWLEDGEMENTS

Part of the research was supported by the Technology Agency of the Czech Republic under project no. ZETA2-TJ02000140. The authors appreciate this support.

7 REFERENCES

ACI 318-14 (2014), Building Code Requirements for Structural Concrete and Commentary, American Concrete Institute; Farmington Hills, Michigan, U.S.A.

Barley, A. D. (1997). The single bore multiple anchor system. *Ground anchorages and anchored structures: Proceedings of the international conference organized by the Institution of Civil Engineers and held in London, UK, on 20–21 March 1997*, 65-75. Thomas Telford Publishing.

Bohn, C., Lopes dos Santos, A., and Frank, R. 2017. Development of axial pile load transfer curves based on instrumented load tests. *Journal of Geotech. and Geoenv. Engineering*. 143(1).

Burland, J. 1973. Shaft friction of piles in clay - a simple fundamental approach. *Publication of: Ground Engineering/UK/*. 6(3).

CEB-FIP Model Code (1990), Design Code (1993), Comite EuroInternational Du Beton.

Dias, T. G. S., and Bezuijen, A. 2018. Load-transfer method for piles under axial loading and unloading. *Journal of Geotechnical and Geoenvironmental Engineering*. 144(1), 04017096.

Dietmar, A. 2020. *Forschungsprojekt Unteres Hausfel (FPUH) - Forschungsbericht*. TU Vienna, Institute of Geotechnics.

Goldberg, D. E. 1989. *Genetic Algorithms in Search, Optimization & Machine Learning*. Addison-Wesley Publishing Company, Inc., 1989. ISBN 0-201-15767-5

Chalmovsky, J., and Mica, L. 2020. Prediction of the load-displacement response of ground anchors via the load-transfer method. *Geomechanics and Engineering*. 20(4), 359-370.

Chalmovský, J. 2024. Optimization of Load-transfer Functions for a Large-diameter Pile in Multi-layered Geological Conditions via a Stochastic Search Algorithm. *Periodica Polytechnica Civil Engineering*. 69(1), 136-145.

Kraft Jr, L. M., Ray, R. P., and Kagawa, T. 1981. Theoretical t-z curves. *Journal of the Geotechnical Engineering Division.* 107(11), 1543-1561.

Lehane, B. M., Gaudin, C., and Schneider, J. A. 2005. Scale effects on tension capacity for rough piles buried in dense sand. *Géotechnique*. 55(10), 709-719.

Ostermayer, H. (1975). PAPER 18 Construction, carrying behaviour and creep characteristics of ground anchors. *Diaphragm Walls & Anchorages*, 141-151. Thomas Telford Publishing.

Randolph, M. F., and Wroth, C. P. (1978). Analysis of deformation of vertically loaded piles. *Journal of the geotechnical engineering division*. 104(12), 1465-1488.

Reddy, E. S. B., O'Reilly, M., and Chapman, D. 1997. A software to predict the behaviour of tension piles. *Computers & structures*. 62(4), 653-658.

Reddy, E. S. B., O'Reilly, M., and Chapman, D. N. 1998. Modified T–Z model - a software for tension piles. *Computers & structures*. 68(6), 613-625.

Seed, H. B., and Reese, L. C. 1957. The action of soft clay along friction piles. *Transactions of the American Society of Civil Engineers*. 122(1), 731-754.

Sulaiman, I. H., and Coyle, H. M. 1976. Uplift resistance of piles in sand. *Journal of the Geotec. Eng. Division*. 102(5), 559-562.

Sutman, M., Olgun, C. G., and Laloui, L. 2019. Cyclic load–transfer approach for the analysis of energy piles. *Journal of Geotechnical and Geoenvironmental Engineering*, 145(1).

Vukotić, G., González Galindo, J., and Soriano, A. 2013. The influence of bond stress distribution on ground anchor fixed length design. Field trial results and proposal for design methodology. *Proc. of the 18th ICSMGE,* Paris.

Wu, Y. D., Liu, J., and Chen, R. 2015. An analytical analysis of a single axially-loaded pile using a nonlinear softening model. *Geomechanics & engineering*. 8(6), 769-781.

Wu, J. J., Cheng, Q. G., Wen, H., Wang, L. J., Li, Y., and Zhang, J. L. 2016. A load transfer approach to rectangular closed diaphragm walls. *Proceedings of the Institution of Civil Engineers-Geotechnical Engineering*, 169(6), 509-526.

Zhang, Q. Q., and Zhang, Z. M. 2012. A simplified nonlinear approach for single pile settlement analysis. *Canadian Geotechnical Journal*. 49(11), 1256-1266.

Zhang, Q. Q., Li, S. C., Liang, F. Y., Yang, M., and Zhang, Q. (2014). Simplified method for settlement prediction of single pile and pile group using a hyperbolic model. *International Journal of Civil Engineering*. 12, 179-192.